Quantum Control of NaI Photodissociation Reaction Product States by Ultrafast Tailored Light Pulses

Christopher J. Bardeen, Jianwei Che, Kent R. Wilson,* and Vladislav V. Yakovlev

Department of Chemistry and Biochemistry, University of California, San Diego, La Jolla, California 92093-0339

Peijun Cong

Department of Chemistry, Hong Kong University of Science and Technology, Kowloon, Hong Kong

Bern Kohler

Department of Chemistry, The Ohio State University, Columbus, Ohio 43210

Jeffrey L. Krause

University of Florida, Quantum Theory Project, P.O. Box 118435, Gainesville, Florida 32611-8435

Michael Messina

Department of Chemistry, University of North Carolina—Wilmington, Wilmington, North Carolina 28403-3297

Received: January 15, 1997[⊗]

Recent experiments by Herek, Materny and Zewail [*Chem. Phys. Lett.* **1994**, *228*, 15] have demonstrated that the timing between two transform-limited, ultrafast laser pulses can be used to control the branching ratio of Na* (electronically excited atomic sodium) to Na in the photodissociation of NaI. In this work, we theoretically show that, by varying the linear chirp of the first pulse without changing its power spectrum or field strength versus time, the Na* to Na branching ratio can be controlled over a large range with a fixed interpulse delay time and a fixed form of the second pulse. Theory predicts that at 0 K the branching ratio can be varied by a factor of 3, while at high temperatures (1000 K), the factor drops to approximately 1.2 due to the effect of the wide distribution of initial states. Experimental results at 1000 K are presented and are found to be consistent with theory. Several possible experimental methods are discussed to overcome the effects of the thermal distribution of initial states.

I. Introduction

Product state selective quantum control was predicted theoretically 10 years ago and is now an experimental reality[1−57]. Two different approaches have been suggested and implemented. One relies on the the quantum mechanical interference between two pathways to the same final state.[7,32] The second uses optimal control to design the laser pulse that best drives matter to a desired target, or goal.[2−4,8−11,28,35] An alternative approach using incoherent interference has also been demonstrated in recent experiments.[34] To focus the discussion, we consider the approaches to quantum control employed in two recent experiments by Zhu et al.,[45] and Herek et al.[54]

Zhu et al.[45] used a combination of a one-photon pathway and a three-photon pathway to selectively control a bound to continuum transition in HI. They demonstrated that the distribution of the products of the photochemical reaction can be controlled by varying the relative phases between these two pathways. This experiment is an example of the theoretical predictions of Brumer and Shapiro[5−7] stating that selective quantum control can be realized by inducing a quantum interference between two pathways to the same degenerate final state.

Herek et al.[54] used ultrafast laser pulses to preferentially select between two possible product channels in NaI. The three potential energy surfaces (PES)[54,58−60] involved in their experiment are shown in Figure 1. A first ultrafast laser pulse, denoted $E_1(t)$ in Figure 1, is used to excite the NaI wave packet from the ground ionic state to a higher lying neutral state. A second ultrafast pulse, denoted by $E_2(t)$ in Figure 1, delayed with respect to the first pulse, then excites the evolving NaI wave packet on

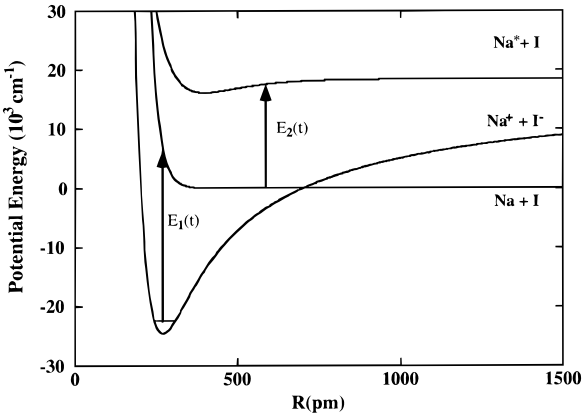

Figure 1. The three potential energy surfaces of NaI involved in the simulations and control experiment and simulations presented in this work. The arrow that points from the ground ionic state to the neutral state represents the action of the chirped localization field E_1 (t). The arrow that points from the neutral state to the final Na* + I state represents the action of the second, locking pulse E_2 (t).

[⊗] Abstract published in *Advance ACS Abstracts,* April 15, 1997.

S1089-5639(97)00219-3 CCC: $14.00

the neutral state to the third electronic state, the Na* + I product state. By detecting both the Na* fluorescence and the free Na produced (using a third pulse), Herek et al.[54] showed that the branching ratio of Na* to Na can be controlled by varying the time delay between the first two pulses. Their experiment demonstrated that the timing of ultrafast light pulses can be used to alter the quantum dynamics and thus the products of a chemical reaction.[4,8,29,37] A different method of controlling the amount of population on the first excited state of NaI (which does not produce Na*) using a two-pulse interference effect has been suggested by Metiu et al.[61,62]

In the present paper (and in a previous brief report[56]) we investigate an alternative way to achieve product control in NaI. The experimental results of Herek et al.[54] clearly illustrated that the timing between two ultrafast light pulses is a powerful knob that one can turn to gain chemical selectivity. Recent experiments and theory performed by our group have pointed to the existence of another knob: the linear chirp of an ultrafast light pulse.[15,16,23,56] We have demonstrated in both gas[15,16] and condensed[23,56] phases that chirped light pulses can be used to control the localization of vibrational wave packets on an electronically excited potential surface. In particular, we showed that I_2 in its ground state can be excited to the electronic B state using a chirped light pulse that is specially tailored to focus a vibrational wave packet about a chosen internuclear distance and internuclear momentum at a chosen time.[16,23,49] A second pulse then excites this wave packet to a final electronic state and laser-induced fluorescence (LIF) is collected as a function of delay time between the pump pulse and the probe pulse. When the sign of the chirp is changed, the relative peak heights in the LIF signal are also changed. Since the collected LIF signal is proportional to the population excited from the B state to the final state, this experiment raises the possibility that the chirp of the pump pulse can be used to induce chemical selectivity.[50] For example, if the probe pulse is tuned to a dissociative state, rather than to a bound state, control of asymptotic products should be possible. By modifying the chirp of the pump pulse, a pump−probe experiment can also be thought of as a control experiment where the LIF is proportional to the product yield. We note that, while a single interaction with light can temporarily localize a wave packet, a second interaction with light is required to permanently "lock in" asymptotic control of the products of a chemical reaction.[33] Thus, in what follows, we will refer to the first pulse as the "localization" pulse and the second pulse as the "locking" pulse, instead of the "pump" and "probe" pulses, respectively.

An integral component of wave packet focusing experiments is the ability to accurately predict the light field required to induce the required localization. We have previously presented a Liouville space theory for the prediction of these tailored fields.[11−13,18,−26] For systems containing many degrees of freedom, we have developed a set of approximations to the exact theory including nearly classical (NC) dynamics,[11,14,23] semiclassical Gaussian wave packet dynamics (GWP),[19,22] time-dependent Hartree (TDH),[20] and stochastic bath (SB) treatments.[12,27] The calculated LIF signals arising from an application of the locking field can also be expressed within each of these approximation schemes.[14,17,22,23,26,63] We stress that, although the localization pulses discussed in this paper are simple chirped pulses, the theory is quite general and does not impose the chirped form a priori.

In this work, we compute the dynamics and the observed LIF signal using both exact quantum dynamics and the nearly classical approximation, which has the advantage that it is numerically much faster for mixed state thermal systems with a wide distribution of initial states and that it can be extended to systems with many degrees of freedom.[23,56] The goal of this paper is to demonstrate that modifying the chirp of an ultrafast light pulse can be an effective route to chemical selectivity. We study the same system as Herek et al.,[54] with the modification that the localization pulse is specifically tailored to drive an evolving localized vibrational wave packet on the neutral state of NaI to a selected location at a selected time. This localized vibrational wave packet is designed to be more susceptible to promotion to the Na* + I state by the second, locking laser pulse (see Figure 2). Thus it is expected that the tailored localization pulse will cause more Na* production than an arbitrary, nonoptimal pump pulse. The population on the neutral state which is not promoted to the Na* + I state will eventually dissociate to Na + I as it oscillates back and forth and leaks through the crossing region.[54,58,59]

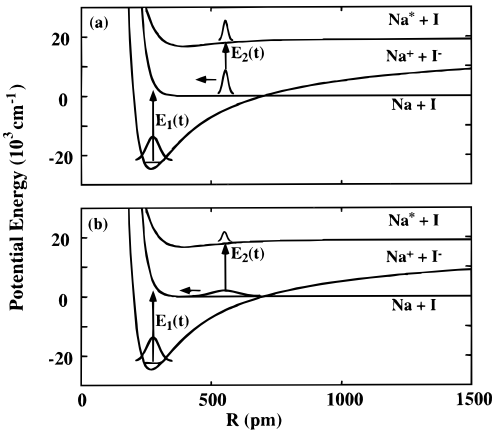

Figure 2. A sketch of the physical picture of chirped pulse localization control in the NaI system. In part a we show the wave packet that is created on the neutral state by a pump field that localizes the NaI vibrational wave packet (a negatively chirped ultrafast light pulse) and the wave packet that is created on the Na* + I state by the application of the second (transform-limited) pulse which locks in the product distribution. In part b we show the wave packet that is created on the neutral state by a pump field that delocalizes the NaI vibrational wave packet (a positively chirped pulse) and the wave packet that is created on the Na* + I state by application of the second (transform limited) locking pulse.

Figure 2 sketches the physical picture involved in using a chirped pump pulse to localize wave packets in NaI and control the products. Part a shows the wave packet created on the neutral state by a negatively chirped, ultrafast localization pulse. Also shown in the figure is the wave packet on the Na* + I state resulting from application of a transform limited locking pulse. Part b shows the results from a positively chirped localization pulse and a transform-limited locking pulse. As can be seen in the figure, the negatively chirped pulse produces a localized wave packet on the neutral state, while the positively chirped pulse produces a delocalized wave packet. The amount of population promoted by the locking pulse to the third state, which dissociates to produce Na*, depends on the shape of the wave packet. The best possible scenario is when the locking pulse interacts with a focused wave packet when it is in the region of the PES where the pulse is resonant with the transition frequency between the two excited states. In this case we have the most population placed on the reactive third state, and thus the most Na* produced. This results in the highest absolute value of the detected LIF signal. There is an interplay between pulse delay and chirp: the optimal solution has both the correct delay of the locking pulse and the correct chirp of the localization pulse. If we look at other pulse delays, the largest LIF signal may not correspond to a negative chirp. A

delocalized wave packet would yield a LIF signal at a delay where a sharper wave packet would show nothing. Figure 2 demonstrates that the magnitude and sign of the linear chirp of the pump field, in addition to the interpulse delay time, are control parameters that can be used to tune the Na* to Na branching ratio. Both the pulse delay time and the pulse chirp will affect the yield of Na* and the optimum chirp will depend on the interpulse delay, and vice versa. From the above arguments, we expect that the best overall combination of the two will be a negatively chirped localization pulse to focus the wave packet, with the locking pulse at the appropriate delay to put as much of this population on the dissociative state as possible.[24,26]

Systems with a narrow distribution of initial states are ideal candidates for successful quantum control. Systems at higher temperatures, with wider thermal distributions of initial states, are in general more difficult to effectively drive to a desired final state because a light field that is optimal for a particular initial state in the distribution, is not, in general, effective for a different initial state. From these arguments, it is expected that the controllability of the system will decrease with increasing temperature.[31,38] This conclusion is supported by the calculations and experiments presented here for NaI. Simulation of the NaI system at 0 K (narrow thermal distribution) shows large control of the product Na*/Na photochemical branching ratio, while simulation of the NaI system at 1000 K (wide thermal distribution) shows weak control. Experiments performed at ~1000 K are in qualitative agreement with the theory and show little control at this temperature. Reduction of the width of the initial quantum distribution can, in principle, be accomplished by cooling the sample in a cryogenic matrix,[23,56] or via expansion in a molecular beam. Another possibility is to use a preparation step, for example another light pulse to project out a narrower distribution of eigenstates, before applying the control pulse.

This paper is organized as follows: In section II we discuss the theory for quantum control of the NaI system and its relation to the experimental observable, the LIF signal. Section III presents results of the simulations for NaI with both narrow and wide initial thermal distributions, and section IV describes the apparatus and experimental results. Finally, in section V we discuss the results and conclusions.

II. Theory

A. Potential Energy Surfaces and Nonadiabatic Coupling. Figure 1 shows the three potential energy surfaces involved in the calculations. The nonadiabatic molecular Hamiltonian $\hat{H}_{NA}^{M}$ for the first two states is written as the following 2 × 2 matrix in the basis of the ionic and neutral electronic state ket vectors $|I\rangle$ and $|N\rangle$,

$$\hat{H}_{NA}^{M} = \begin{pmatrix} \hat{T} + V_I & g(R) \\ g(R) & \hat{T} + V_N \end{pmatrix} \tag{1}$$

In this equation V_I and V_N are the ionic and neutral potential energy surfaces, respectively, $\hat{T}$ is the kinetic energy operator, and $g(R)$ is the nonadiabatic coupling between the ionic and neutral states. The potential energy surfaces used for the ionic and neutral states have been presented elsewhere.[54,58] The nonadiabatic coupling between the ionic and neutral surfaces is taken to be the following function of the NaI internuclear coordinate R,

$$g(R) = Ae^{-\beta(R-\gamma)^2} \tag{2}$$

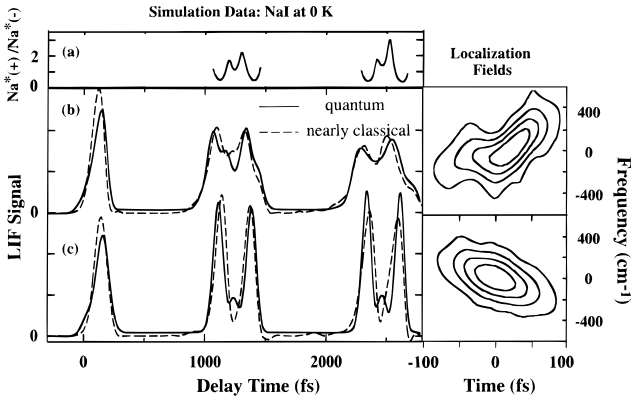

Figure 3. Results of simulations of the LIF signal from a localization field with positive chirp, and negative chirp, parts b and c, respectively, at a temperature of 0 K. The solid and dashed lines in each part are the results of the QD and NC simulations, respectively. Part a shows Na*(+chirp)/Na*(−chirp), the ratio of Na* production for positive and negative chirps at a temperature of 0 K, from the QD calculation. The right-hand parts show the Wigner transforms of the localization fields.

The coupling strength A is 439 cm^{-1}, the width β is 0.007 14 pm^{-2}, and the parameter γ is 693 pm.[58]

For the NC approximation we will find it convenient to perform calculations on the adiabatic states rather than on the coupled nonadiabatic states defined above. The adiabatic molecular Hamiltonian $\hat{H}_{A}^{M}$ is written in terms of the adiabatic state vectors $|\alpha\rangle$ and $|\beta\rangle$ as follows

$$\hat{H}_{A}^{M} = \begin{pmatrix} \hat{T} + V_\alpha & 0 \\ 0 & \hat{T} + V_\beta \end{pmatrix} \tag{3}$$

Here V_α and V_β are the adiabatic potential energy surfaces which are given as the eigenvalues of the following potential matrix,

$$V = \begin{pmatrix} V_I & g(R) \\ g(R) & V_N \end{pmatrix} \tag{4}$$

The complete nonadiabatic Hamiltonian, including the interaction of the molecule with the pump field $E_1(t)$, is

$$\hat{H}_{NA} = \begin{pmatrix} \hat{T} + V_I & g(R) + \mu E_1^*(t) \\ g(R) + \mu E_1(t) & \hat{T} + V_N \end{pmatrix} \tag{5}$$

In the above equation, μ is the transition dipole moment between the ionic and neutral states, which is set equal to a constant (Condon approximation). The final state of Na* + I that is accessed by the locking light field $E_2(t)$ is modeled as a Morse potential,

$$V_f = D_f(1 - e^{-a(R-R_{eq})})^2 \tag{6}$$

The numerical values of the parameters for this potential are D_f = 1863 cm^{-1}, a = 0.008 314 pm^{-1}, and R_{eq} = 397 pm.[64] The interactions of $E_1(t)$ and $E_2(t)$ with the molecular system are treated perturbationally. The accuracy of the theoretical calculations depends on the knowledge of the potential surfaces.[59] While the spectroscopy of the first two electronic states of NaI has been well-studied, much less is known about the structure of the third state. For our calculations we use the most recent parameters derived from time-dependent experiments.[64] The good qualitative agreement between theory and experiment shown in Figures 5 and 6 indicates that we are using representations of the potential energy surfaces satisfactory for the purposes of this paper, although we have not systematically tested the sensitivity of the calculations to changes in the surfaces. More accurate potential energy surfaces could improve

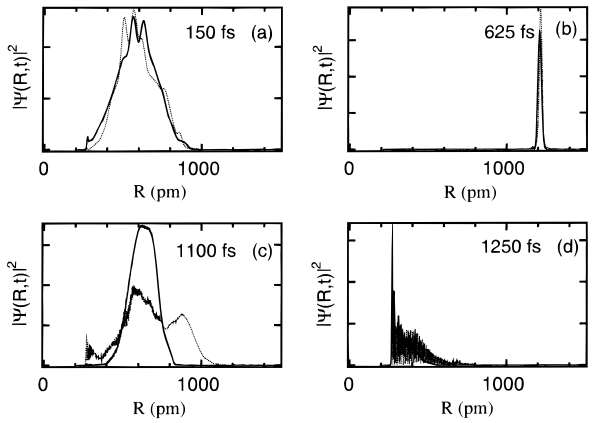

Figure 4. The population distributions on the excited state adiabatic potential energy surface excited with a negatively chirped localization pulse (solid line) and a positively chirped pulse (dashed line). Parts a−d show the wave packets at delays 150, 625, 1100, and 1250 fs after excitation, respectively.

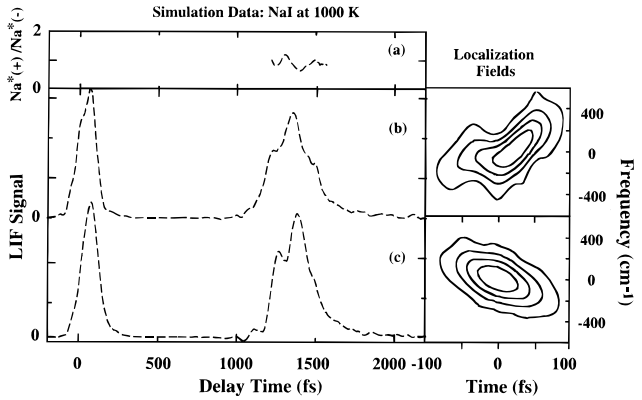

Figure 5. Results of NC simulations of the LIF signal from a localization field with positive chirp and negative chirp, parts b and c, respectively, at a temperature of 1000 K. Part a shows Na*(+chirp)/Na*(−chirp), the ratio of Na* production for positive and negative chirps at a temperature of 1000 K. The right-hand parts show the Wigner transforms of the localization fields.

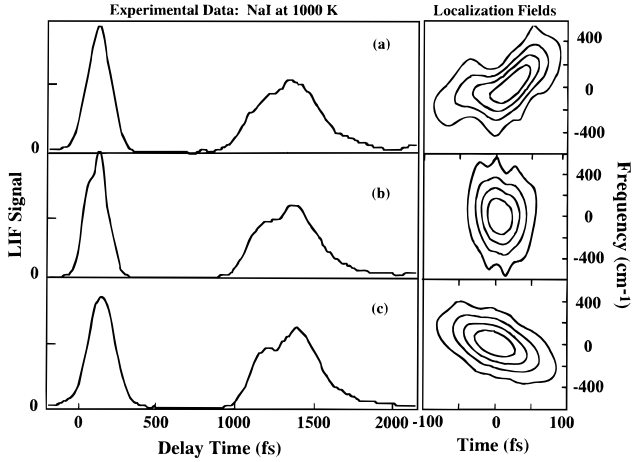

Figure 6. Experimental LIF signals from positively chirped, transform-limited, and negative chirped localization fields, parts a, b, and c, respectively. The right-hand parts show the Wigner transforms of the localization fields.

the agreement between theory and experiment, but would not affect the main conclusions of the paper.

B. Design of the Control Field $E_1(t)$. We now consider the use of optimal control theory to tailor the localization field, $E_1(t)$. The operational ansatz is that a localized wave packet on the neutral state of NaI is more susceptible to a locking pulse that promotes amplitude to a higher lying excited state than a delocalized wave packet.[17,26] The goal, then, is to create a well-localized target[13,24,25] on the neutral state of NaI, centered at a particular internuclear distance R at a particular target time t_f. We define the target as the following minimum uncertainty wave packet,

$$\phi_T(R) = (2\pi w_{RR})^{-1/4} \exp\left[-\frac{1}{4w_{RR}}(R-\bar{R})^2 + \frac{i\bar{p}}{\hbar}(R-\bar{R})\right] \tag{7}$$

The phase space center of this target is specified by $\bar{R}$ and $\bar{p}$, and the target positional width is w_{RR}.

The control field $E_1(t)$ that drives the system to maximum overlap with the target in eq 7 can be computed using optimal control theory. In the weak response (perturbative) regime, we have developed a method to obtain directly the globally optimal field.[12,13] This formulation is particularly efficient since the control fields are determined as the eigenvectors of a specially constructed control kernel. The input to the formulation is the time-evolved wave packet in the absence of the field,[11−13] which can be computed by standard means. In the strong response regime, the control kernel itself depends on the field, so the optimal fields must be determined iteratively.[18,29,36]

For NaI at 0 K, the exact quantum dynamics is quickly computable.[17,23] For NaI, a temperature of about 1000 K is necessary to achieve appreciable vapor pressure for an experiment. At this temperature, the gas phase NaI molecules have a wide distribution of initial states, and so we must average the system dynamics for control calculations over the initial thermal distribution. We use the NC method (averaging over exact quantum mechanics being numerically very lengthy) to compute the system evolution via the adiabatic molecular Hamiltonian. The formalism for the NC approach to quantum control has been described in detail elsewhere.[11,14,23] The NC method used here involves a set of approximations[23] including a quantum corrected initial distribution of positions and momenta, a causality preserving interaction with the light pulses, and an approximate propagation of the quantum density matrix by a swarm of classical trajectories. The relative phases of the classical trajectories are preserved in the calculations. At 1000 K, we will use the results of the NC algorithm to predict the optimal fields and to simulate the the LIF signal, which is an experimental signature of control.[17,26]

C. The Observable: the LIF Signal. As described in the introduction, population is created on the dissociative Na* + I state by the application of a locking pulse that intercepts a wave packet evolving on the neutral state. The experimental observable is the LIF signal resulting from fluorescence from the Na* product as a function of the delay time between the localization pulse and the locking pulse. The signal is proportional to the amount of population that is excited to the final Na* state. To compare theory to experiment, we must simulate the experimentally measured LIF signal. Since the experiment is performed at a temperature of 1000 K, we must include the effects of the thermal distribution on the dynamics and the experimental signal.

The NC approximation to the LIF signal, which is discussed in detail elsewhere,[23] is obtained from the following semiclassical expression for the signal,

$$S(t_d) \approx \int_{-\infty}^{\infty} dt\, \mathrm{Tr}[|\mu_{f\beta}|^2 I_T(U_{f\beta},t)\rho_e(t+t_d)] \tag{8}$$

where $I_T(U_{f\beta},t)$ is the causality transform of the locking pulse defined as[63]

$$I_T(\omega,t) \equiv 2\mathrm{Re}\,[E_2^*(t)\int_0^\infty \mathrm{d}t' \mathrm{e}^{i(\omega'-\Omega_T)t'} E_2(t+t')] \qquad (9)$$

Here $U_{f\beta}$ is defined as $U_{f\beta} \equiv (V_f - V_\beta)/\hbar$, with V_f and V_β defined in eqs 6 and 3, respectively, $E_2(t)$ is the locking pulse, and Ω_T is the carrier frequency of the locking pulse. In eq 8, $\mu_{f\beta}$ is the transition dipole moment between the adiabatic state V_β and the final state. $\mu_{f\beta}$ is calculated by diagonalizing the 3-level Hamiltonian (ionic, neutral, and the final states) in the presence of the locking pulse.

$$\mu_{f\beta} = \mu_{fN}\frac{V_N - V_I + \sqrt{(V_N - V_I)^2 + 4g^2}}{\sqrt{4g^2 + [V_N - V_I + \sqrt{(V_N - V_I)^2 + 4g^2}]^2}} \qquad (10)$$

Here, μ_{fN} is the transition dipole moment between the intermediate neutral state and the final state, and is assumed to be a constant in our calculations. The coupling function g is defined in eq 2. Note that this effective transition dipole for the adiabatic state goes to zero after the crossing point (i.e., as the coupling constant g goes to zero) since for large internuclear distances the ionic potential is at higher energy than the neutral state and the numerator goes to zero. The physical reason that the transition dipole between the adiabatic state and the final state disappears at large internuclear distances is that at these distances the adiabatic state is largely ionic, while the final state is covalent. A transition between the two would involve an electron transfer over a large distance in the gas phase, which is very unlikely. Within the NC approximation, we can write $\rho_e(t)$, the time evolved density matrix on the neutral state of NaI, as

$$\rho_e(t,R,R) = \frac{1}{N}\sum_i \delta[R - R_i(t)] \qquad (11)$$

where the sum runs over all the phase space trajectories of the ensemble, $R_i(t)$ is the ith trajectory, and N is the total number of trajectories. The classical phase space trajectories are performed on the adiabatic surfaces defined in eq 4.

III. Simulation Results

We now present results of the simulation of quantum control of the Na* to Na branching ratio. The simulations allow us to easily compare and contrast the controllability of the NaI system under two quite different conditions. The first is control of NaI molecules prepared with the narrowest possible initial eigenenergy distribution at a temperature of 0 K. The second is control of molecules at 1000 K, a temperature approximately corresponding to our experimental measurements, in which a wide distribution of initial states is encountered.

As we mentioned above, the control scenario involves creating a focused (defocused) wave packet on the neutral surface of NaI such that the wave packet is more (less) susceptible to promotion by the locking pulse. We must choose a target time, the time at which we best attain the intermediate target state, defined as the minimum uncertainty wave packet in eq 7. We choose this target time to correspond to the interval during which the NaI wave packet on the neutral state is making its first return trip toward the inner turning point and passes through the internuclear distance at which the difference between the potentials corresponds to the average photon energy of the locking pulse. The target in this case is a molecular reflectron[13] since the wave packet must localize after reflecting from the outer turning point of the potential and thus has an overall negative value of the momentum (that is, the Na and I atoms are moving toward each other). The position of the focused wave packet is chosen to be at $\bar{R} = 590$ pm, where it can be accessed by the locking pulse. The choice of where the wave packet focuses is somewhat arbitrary, and we may choose to focus the wave packet elsewhere on the PES. It is worth noting that the wave packet undergoes a natural sharpening at the far turning point of the adiabatic well (where the transition dipole to the final state is essentially zero), and by using chirped light fields we can now make the wave packet focus at other points on the PES as well.

We find that both the quantum dynamics (QD) and NC simulations predict that the globally optimal localization field that best creates the reflectron target has an overall negative linear chirp. The fields predicted from both approaches are quite similar.[14] In the simulations we do not use the exact calculated optimal fields, but we use instead the experimental pump fields that are the best approximations to the theoretical predictions which we were able to create and measure. The locking fields used in the simulations are also the experimentally measured probe fields. This allows the simulations to be directly compared to experiment and assures that the fields are experimentally realizable. The angle between the polarization vectors of the localization and locking pulses in all calculations is set to 0° to match the experimental configuration, and we assume that both transitions are parallel in symmetry.

A. Narrow Thermal Distribution. Figure 3 shows the results of simulations of the LIF signal resulting from localization fields with a positive chirp and a negative chirp at a temperature of 0 K. The solid lines and dashed lines in each part are the results of the QD and NC calculations, respectively. The parts on the right hand side of Figure 3 show the Wigner transforms of the localization fields. The positively and negatively chirped fields are nearly a matched pair in the sense that both fields have nearly the same power spectrum and field strength, and thus the fields mainly differ only in the time ordering of the frequencies. The detailed shape of the signals has been discussed by many previous workers,[58,59,65,64] and here we only give a brief outline of how the observed LIF corresponds to the wave packet motion on the adiabatic surface. The spectrum of the locking pulse defines a window, through which the wave packet periodically travels and where it is excited to the third state. The first peak around zero delay time in the LIF signal corresponds to the outgoing wave packet passing through the locking pulse window, and the double peaks at longer delay times correspond to the double passing through the locking window (i.e, incoming and outgoing), since the window is not at a turning point. The first characteristic to notice in Figure 3 is the similarity between the QD and NC calculations of the LIF signal, which gives added confidence to the NC approximation which can be used to extend quantum control calculations to large molecules and condensed phase systems where exact quantum calculation are impractical, as well as to high-temperature systems, where they can be computationally challenging. Second, the LIF signal resulting from the negatively chirped localization field is significantly different than that arising from the positively chirped field. The main result of the chirp is to change the width and relative intensity of the peaks, since the negatively chirped pulse produces a narrow wave packet in the probe region, while a positively chirped pulse yields a wider wave packet.

We further investigate the effect of pulse chirp on wave packet motion in Figure 4, where we plot the quantum mechanical probability distributions due to both negative and positive chirp excitations at various delays. Part a shows the excited state wave packet 150 fs after the localization pulse,

during its first pass through the locking pulse window. This early wave packet is obviously very similar for both positively and negatively chirped localization pulses. The wave packet at the outer turning point, shown in part b, is also very similar for either pulse, and it is also very focused due to the natural turning point dynamics. Unfortunately, as mentioned above, we cannot take advantage of this natural focusing due to the lack of oscillator strength in this region. Part c shows the wave packet at the target time of 1100 fs. Both positive and negative chirps have resulted in wave packets centered at 590 pm, but the wave packet created by a negatively chirped pulse is much more localized and overlaps with the finite width of the locking pulse better. Finally, part d shows the wave packets at the inner turning point of the PES, after one full period of oscillation. From these "snapshots" of the calculated wave packets, we see that the experimentally measured chirped pulses give rise to either a relatively narrow wave packet, localized on the PES, or to a more diffuse structure, which has substantial amplitude outside the locking pulse window. The form of the wave packet at subsequent oscillations is very similar to that shown in Figure 4, which is to say that the focusing is periodic.

The top part in Figure 3 shows Na*(+chirp)/Na*(−chirp), the ratio of Na* produced with the positive chirp to that produced with the negative chirp. The amount of Na* produced at a given delay is directly proportional to the population in the locking window at that delay. The figure shows that the production of Na* can be enhanced by approximately a factor of 3 by using a positively versus a negatively chirped pulse for a given interpulse delay, i.e., 2600 fs. This enhancement in the ratio is due to the broader wave packet (produced by positive chirps) giving LIF signal at delays where the sharper wave packet (produced by negative chirps) is completely outside the spectral window of the locking pulse. While the positively chirped pulse may yield significant enhancement for some locking pulse delays, the largest peak signal results from a negatively chirped pulse when the wave packet is focused in the region where most of it can be excited to produce Na*. The delay at which this maximum LIF signal is observed, around 1100 fs, corresponds to the target time used in the optimal control calculations. When both the delay and the chirp are free parameters, the largest yield of Na* results from a negatively chirped pump pulse, in agreement with the reasoning in the introduction. It is interesting to note that if one fixes the interpulse delay, then the best way to enhance the Na* yield may be either a positively or negatively chirped pulse, as can be seen by the delay dependence of the ratio. This clearly demonstrates that the tailoring of the localization pulse, in the form of its chirp, can be an important control parameter, in addition to the delay time between the pulses.

B. Wide Thermal Distribution. Figure 5 shows NC theoretical results for NaI at a temperature of 1000 K. Comparing Figures 3 and 5, we see that the contrast between the LIF signals that result from the positively and negatively chirped localization pulses is not nearly as large for the high temperature case as for the 0 K case. The main difference in the spectra is that the peaks are much broader at higher temperature. Not surprisingly, control is more difficult for the wider initial thermal distributions of NaI molecules, because wave packet localization is less effective. The top part in Figure 5 shows the Na*-(+chirp)/Na*(−chirp) ratio and illustrates the degradation in the control of Na* to Na production for a wide NaI thermal distribution (∼1.2) as compared to the narrow distribution (∼3). In these NC simulations, 2000 trajectories are used in each case.

The wide thermal distribution of initial NaI rovibrational states diminishes the degree of control because no single light field can efficiently drive all the initial rovibrational states onto the same target state. There are several reasons why differing initial rovibrational states in the NaI molecular ensemble will evolve differently when excited by the same tailored light field.[48,66] First, different initial rovibrational states can be excited to different portions of the neutral NaI potential energy surface. Second, rotation−vibration centrifugal coupling, which is dependent on *J*, the angular momentum quantum number, will cause each rovibrational state in the NaI ensemble (even those belonging to the same vibrational level) to experience different forces and thus exhibit different dynamics. Lastly, there is an evolution of the orientational distribution of the NaI molecules,[23] which also affects the rotational distribution. This last effect on the LIF signal can be removed by setting the angle between the polarizations of the two pulses to the "magic angle".[67]

IV. Experimental Section

A. Experimental Design. The experimental apparatus is similar to that used previously in demonstrations of wave-packet control in gas phase I_2.[15,16,23] Briefly, the laser system consists of a Ti:Sapphire oscillator whose output is regeneratively amplified to the millijoule level. These near infrared pulses are then used to pump a continuum-seeded optical parametric amplifier,[68,69] whose output is frequency-doubled to generate the locking pulses in the visible region. A fraction of these pulses is then frequency-doubled to provide the UV localization pulses. Both localization and locking pulses travel through sets of prisms to compensate for material dispersion in the beam paths. By translating a prism in the localization beam in a direction perpendicular to the beam path, we can control the amount of dispersion that the beam experiences and thus control the chirp of the pulse. For the experiments reported here, the localization pulses have a bandwidth of about 400 cm^{-1} centered at 310 nm, while the locking pulses have a bandwidth of about 800 cm^{-1} centered at 620 nm. A slit is placed in the prism sequence of the locking pulses to filter out wavelengths shorter than 590 nm in order to prevent background signal from free Na absorption. The decrease in bandwidth from locking to localization pulses is caused by the 0.3 mm thick LBO doubling crystal used to generate the localization pulses. The localization pulses are approximately 50 fs in duration when the prisms are optimally positioned for minimum pulse duration, while the locking pulses are about 35 fs. The localization and locking pulse electric field (polarization) vectors are set to be parallel to each other. Care is taken to precompensate for dispersive material in the beam (optics and oven and gas cell windows) so that the laser pulses are of the correct duration when they enter the NaI cell.

Both pulse trains are focused into a cell containing the NaI vapor, which is generated by heating a quartz cell in an oven in a manner similar to that used by Herek et al.[54] The temperature of the cell is measured using a thermocouple probe and is in the range of 900−1000 K. The LIF at 589 nm originating from the Na* species is detected by collecting the scattered light at 90° to the laser beams and imaging it onto a photomultiplier tube whose output is sent to a boxcar and then to a computer.

The characterization of the optical pulses is accomplished using the frequency resolved optical gating (FROG) technique.[70,71] The pulse to be characterized is split into two identical pulses, one of which acts as a polarization gate for the other in a 1 mm thick plate of fused silica, which serves as the Kerr medium. The wavelength-resolved transmittance of the other beam is detected using a CCD array as a function of

the delay between the two pulses, and this two-dimensional data set is analyzed using a numerical algorithm to derive the electric field $E(t)$ of the light pulse. We have found this method to be fairly accurate with respect to reproducing the independently measured power spectrum and intensity autocorrelation function of the pulse. A convenient way to represent the recovered complex electric field is by using the Wigner transform to create a two-dimensional plot of the intensity of the field as a function of both time and frequency. In such a plot, a positively chirped pulse, in which the lower frequencies precede the higher frequencies in time, appears as set of contours with an overall positive slope. A negatively chirped pulse has the opposite slope, while a transform-limited pulse has no slope. The fwhm pulse widths are 99 and 96 fs for the positively and negatively chirped pulses, respectively.

B. Experimental Results. Figure 6 shows the experimental LIF signals for the NaI control experiment. Parts a, b, and c show the LIF signals resulting from positively chirped, transform-limited, and negatively chirped pump (localization) fields, respectively. In the right hand parts of Figure 6 we show the Wigner transforms of the pump fields. The data are in qualitative agreement with the simulated results in Figure 5, with roughly similar variations of the peak heights in the 1200 to 1700 fs region. The control is fairly weak, as expected from the simulations at 1000 K. The main effect in both the high-temperature simulations and the experimental data is the slight enhancement, with negative chirp, of the peak at about 1200 fs which corresponds to the reflectron wave packet. The peak is larger than both the positively chirped and transform limited pulse signals and indicates that a negatively chirped pulse is producing some focusing of the wave packet. While the low-temperature theory also showed an enhancement for subsequent oscillations in the LIF , these are not observed experimentally at 1000 K since for larger pulse delays the wide thermal distribution washes out the chirp effect even more. We can expect the experimental product branching ratios to show similar variations to those seen in Figure 5.

V. Discussion and Conclusions

We wish to emphasize three major points in this work. First, we have illustrated theoretically that it is possible to control the product yield in a chemical reaction using specially tailored ultrafast light fields. The reaction considered here is a simple photodissociation reaction, and the product is an electronically excited atom, but we believe that the procedure presented here is quite general. Second, we have also shown that the tailoring can have the form of a simple chirp of an ultrafast light pulse and that this can be sufficient to induce chemical selectivity. We emphasize that this simple chirp is the optimal solution given the chosen target and the molecular PES, and was not an a priori assumption. The chirp provides the ability to exert control beyond tuning the frequency and relative delay of the localization and locking pulses. As we have demonstrated, a matched pair of chirped pulses, each of which has essentially the same power spectrum and field strength versus time and differs only in its correlation of frequency versus time, can produce dramatically different product yields. One must keep in mind that there is an interplay between pulse delay and pulse chirp. From Figure 3 it is clear that the chirp that optimizes the Na* yield for a given delay may be either positive or negative. For the largest possible yield of Na*, however, it is clear that a negatively chirped pulse will place the most population in the locking pulse window for excitation to the product state. Figure 3 shows that the largest signal overall occurs for a negatively chirped pulse at the appropriate delay. Finally, we have illustrated the detrimental effects that a large thermal distribution can have on controllability. Our simulations predict a large degree of quantum control with a narrow distribution of initial NaI rovibrational states. However, this effect is considerably diminished, as seen both theoretically and experimentally, when the temperature of the system is increased to ~1000 K.

The deleterious effect of wide thermal distributions (which we expect in general will make quantum control more difficult) can, in principle, be ameliorated in several ways. One can cool the sample by, for example, expanding NaI in a molecular beam, or by embedding the molecular system in a cold inert medium such as a rare gas matrix.[21−23,56] We are presently planning such experiments. Alternatively, one might project out a narrow distribution of initial states by manipulating the sample with a preparatory light pulse or multiple light pulses. It is also intriguing to speculate whether the quantum control at higher temperature might be improved by moving to the strong response regime,[18] or by using more complicated pulse shapes. One point to keep in mind is that the thermal distribution results in a distribution of initial conditions for the quantum control problem, and it is not clear that a single light field exists that will be the optimal solution for each condition. One approach that could be tried is to use a feedback loop to control the pulse shaping and let a computer algorithm optimize the Na* fluorescence signal, independent of any calculations.[72,73] Such an experiment should be possible given existing laser technology.

References and Notes

(1) Zewail, A. H. *Phys. Today* **1980**, *33*, 27.
(2) Warren, W. S.; Rabitz, H.; Dahleh, M. *Science* **1993**, *259*, 1581.
(3) Tannor, D. J.; Rice, S. A. *Adv. Chem. Phys.* **1988**, *70*, 441.
(4) Rice, S. A. *Science* **1992**, *258*, 412.
(5) Brumer, P.; Shapiro, M. *Acc. Chem. Res.* **1989**, *22*, 407.
(6) Brumer, P.; Shapiro, M. *Annu. Rev. Phys. Chem.* **1992**, *43*, 257.
(7) Shapiro, M.; Brumer, P. *Int. Rev. Phys. Chem.* **1994**, *13*, 187.
(8) Rabitz, H.; Shi, S. *Adv. Molec. Vib. Collision Dyn.* **1991**, *1A*, 187.
(9) Weiner, A. M.; Leaird, D. E.; Wiederrecht, G. P.; Nelson, K. A. *Science* **1990**, *247*, 1317.
(10) Kohler, B.; Krause, J.; Raksi, F.; Wilson, K. R.; Whitnell, R. M.; Yakovlev, V. V.; Yan, Y. J. *Acc. Chem. Res.* **1995**, *28*, 133.
(11) Krause, J. L.; Whitnell, R. M.; Wilson, K. R.; Yan, Y. J. In *Femtosecond Chemistry*; Manz, J., Wöste, L., Eds.; Springer-Verlag: Weinheim, 1995; p 743.
(12) Yan, Y. J.; Gillilan, R. E.; Whitnell, R. M.; Wilson, K. R.; Mukamel, S. *J. Phys. Chem.* **1993**, *97*, 2320.
(13) Krause, J. L.; Whitnell, R. M.; Wilson, K. R.; Yan, Y. J.; Mukamel, S. *J. Chem. Phys.* **1993**, *99*, 6562.
(14) Krause, J. L.; Whitnell, R. M.; Wilson, K. R.; Yan, Y. J. In *Ultrafast Reaction Dynamics and Solvent Effects*; Gauduel, Y.; Rossky, P., Eds.; American Institute of Physics: New York, 1994; p 3.
(15) Kohler, B.; Krause, J. L.; Whitnell, R. M.; Wilson, K. R.; Yakovlev, V. V.; Yan, Y. J. In *Ultrafast Phenomena IX*; Mourou, G. A., Zewail, A. H., Barbara, P. F., Knox, W. H., Eds.; Springer-Verlag: Berlin, 1994; p 44.
(16) Kohler, B.; Yakovlev, V. V.; Che, J.; Krause, J. L.; Messina, M.; Wilson, K. R.; Schwentner, N.; Whitnell, R. M.; Yan, Y. J. *Phys. Rev. Lett.* **1995**, *74*, 3360.
(17) Che, J.; Krause, J. L.; Messina, M.; Wilson, K. R.; Yan, Y. J. *J. Phys. Chem.* **1995**, *99*, 14949.
(18) Krause, J. L.; Messina, M.; Wilson, K. R.; Yan, Y. J. *J. Phys. Chem.* **1995**, *99*, 13736.
(19) Messina, M.; Wilson, K. R. *Chem. Phys. Lett.* **1995**, *241*, 502.
(20) Messina, M.; Wilson, K. R.; Krause, J. L. *J. Chem. Phys.* **1996**, *104*, 173.
(21) Che, J.; Messina, M.; Wilson, K. R.; Yan, Y. J. In *Femtochemistry, Ultrafast Chemical and Physical Processes in Molecular Systems*; Chergui, M., Ed.; World Scientific: Signapore, 1996; p 360.
(22) Che, J.; Messina, M.; Wilson, K. R.; Apkarian, V. A.; Li, Z.; Martens, C. C.; Zadoyan, R.; Yan, Y. J. *J. Phys. Chem.* **1996**, *100*, 7873.
(23) Bardeen, C. J.; Che, J.; Wilson, K. R.; Yakovlev, V. V.; Apkarian, V. A.; Martens, C. C.; Zadoyan, R.; Kohler, B.; Messina, M. *J. Chem. Phys.*, submitted for publication.
(24) Cao, J.; Wilson, K. R. *J. Chem. Phys* **1996**, *105*, 5206.

(25) Cao, J.; Wilson, K. R. *Phys. Rev. A.*, in press.
(26) Cao, J.; Wilson, K. R. *J. Chem. Phys.* **1997**, *105*, 5223.
(27) Cao, J.; Wilson, K. R. *J. Chem. Phys.*, submitted for publication.
(28) Tannor, D. J.; Rice, S. A. *J. Chem. Phys.* **1985**, *83*, 5013.
(29) Kosloff, R.; Rice, S. A.; Gaspard, P.; Tersigni, S.; Tannor, D. J. *Chem. Phys.* **1989**, *139*, 201.
(30) Rice, S. A.; Zhao, M. In *Laser Techniques for State-Selected Chemistry II*; Hepburn, J. W., Ed.; SPIE: Bellingham, WA, 1994; Vol. 2124, p 246.
(31) Brumer, P.; Shapiro, M. *Faraday Discuss.* **1986**, *82*, 177.
(32) Shapiro, M.; Brumer, P. *J. Chem. Phys.* **1986**, *84*, 4103.
(33) Brumer, P.; Shapiro, M. *Chem. Phys.* **1989**, *139*, 221.
(34) Shnitman, A.; Sofer, I.; Golub, I.; Yogev, A.; Shapiro, M.; Chen, Z.; Brumer, P. *Phys. Rev. Lett.* **1996**, *76*, 2886.
(35) Peirce, A. P.; Dahleh, M. A.; Rabitz, H. *Phys. Rev. A* **1988**, *37*, 4950.
(36) Shi, S.; Woody, A.; Rabitz, H. *J. Chem. Phys.* **1988**, *88*, 6870.
(37) Shi, S.; Rabitz, H. *Chem. Phys.* **1989**, *139*, 185.
(38) Judson, R. S.; Lehmann, K. K.; Rabitz, H.; Warren, W. S. *J. Mol. Struct.* **1990**, *223*, 425.
(39) Manz, J.; Parmenter, C. S. *Chem. Phys.* **1989**, *139*. 1.
(40) Chen, C.; Yin, Y. Y.; Elliott, D. S. *Phys. Rev. Lett.* **1990**, *64*, 507.
(41) Yin, Y.-Y.; Elliott, D.; Shehadeh, R.; Grant, E. *Chem. Phys. Lett.* **1995**, *241*, 591.
(42) Park, S. M.; Lu, S. P.; Gordon, R. J. *J. Chem. Phys.* **1991**, *94*, 8622.
(43) Kleiman, V. D.; Zhu, L.; Allen, J.; Gordon, R. J. *J. Chem. Phys.* **1995**, *103*, 10800.
(44) Kleiman, V. D.; Zhu, L.; Li, X.; Gordon, R. J. *J. Chem. Phys.* **1995**, *102*, 5863.
(45) Zhu, L.; Kleiman, V.; Li, X.; Lu, S.; Trentleman, K.; Gordon, R. *Science* **1995**, *270*, 77.
(46) Baranova, B. A.; Chudinov, A. N.; Zel'dovich, B. Y. *Opt. Comm.* **1990**, *79*, 116.
(47) Scherer, N. F.; Ruggiero, A. J.; Du, M.; Fleming, G. R. *J. Chem. Phys.* **1990**, *93*, 856.
(48) Scherer, N. F.; Matro, A.; Ziegler, L. D.; Du, M.; Carlson, R. J.; Cina, J. A.; Fleming, G. R. *J. Chem. Phys.* **1992**, *96*, 4180.
(49) Janszky, J.; Adam, P.; Vinogradov, A. V.; Kobayashi, T. *Chem. Phys. Lett.* **1993**, *213*, 368.
(50) Amstrup, B.; Doll, J. D.; Sauerbrey, R. A.; Szabó, G.; Lörincz, A. *Phys. Rev. A* **1993**, *48*, 3830.
(51) Baumert, T.; Gerber, G. *Isr. J. Chem.* **1994**, *34*, 103.
(52) Sugawara, M.; Fujimura, Y. *J. Chem. Phys.* **1994**, *100*, 5646.
(53) Assion, A.; Baumert, T.; Seyfried, V.; Gerber, G. In *Ultrafast Phenomena X*; Fujimoto, J., Zinth, W., Barbara, P. F., Knox, W. H., Eds.; Springer-Verlag: Berlin, 1996; p 190 (in press).
(54) Herek, J. L.; Materny, A.; Zewail, A. H. *Chem. Phys. Lett.* **1994**, *228*, 15.
(55) Apkarian, V. A. In *Femtochemistry, Ultrafast Chemical and Physical Processes in Molecular Systems*; Chergui, M., Ed.; World Scientific: Singapore, 1996; p 603.
(56) Apkarian, V. A.; Bardeen, C. J.; Che, J.; Kohler, B.; Martens, C. C.; Messina, M.; Wilson, K. R.; Yakovlev, V. V.; Zadoyan, R. In *Ultrafast Phenomena X*; Fujimoto, J., Zinth, W., Barbara, P. F., Knox, W. H., Eds.; Springer-Verlag: Berlin, 1996; p 219.
(57) Xing, G. Q.; Wang, X. B.; Huang, X.; Bersohn, R. *J. Chem. Phys.* **1996**, *104*, 826.
(58) Engel, V.; Metiu, H. *J. Chem. Phys.* **1989**, *90*, 6116.
(59) Engel, V.; Metiu, H. *J. Chem. Phys.* **1989**, *91*, 1595.
(60) Benjamin, I.; Wilson, K. R. *J. Phys. Chem.* **1991**, *95*, 3514.
(61) Metiu, H.; Engel, V. *J. Opt. Soc. Am. B* **1990**, *7*, 1709.
(62) Metiu, H.; Engel, V. *Faraday Discuss.* **1991**, *91*, 249.
(63) Yan, Y. J. *Chem. Phys. Lett.* **1992**, *198*, 43.
(64) Cong, P.; Roberts, G.; Herek, J. L.; Mohktari, A.; Zewail, A. H. *J. Phys. Chem.* **1996**, *100*, 7832.
(65) Rose, T. S.; Rosker, M. J.; Zewail, A. H. *J. Chem. Phys.* **1989**, *91*, 7415.
(66) Bavli, R.; Engel, V.; Metiu, H. *J. Chem. Phys.* **1992**, *96*, 2600.
(67) Dantus, M.; Bowman, R. M.; Zewail, A. H. *Nature* **1990**, *343*, 737.
(68) Yakovlev, V. V.; Kohler, B.; Wilson, K. R. *Opt. Lett.* **1994**, *19*, 2000.
(69) Wilson, K. R.; Yakovlev, V. V. *J. Opt. Soc. Am. B* **1997**, *14*, 444.
(70) Trebino, R.; Kane, D. J. *J. Opt. Soc. Am. A* **1993**, *10*, 1101.
(71) Kohler, B.; Yakovlev, V. V.; Wilson, K. R.; Squier, J.; Delong, K. W.; Trebino, R. *Opt. Lett.* **1995**, *20*, 483.
(72) Neuhauser, D.; Rabitz, H. *Acc. Chem. Res.* **1993**, *26*, 496.
(73) Yan, Y. J.; Kohler, B. E.; Gillilan, R. E.; Whitnell, R. M.; Wilson, K. R.; Mukamel, S. In *Ultrafast Phenomena VIII*; Martin, J.-L., Migus, A., Mourou, G. A., Zewail, A. H., Eds.; Springer-Verlag: Berlin, 1993; pp 8−12.